Hindawi
Journal of Applied Mathematics
Volume 2022, Article ID 5384627, 12 pages
https://doi.org/10.1155/2022/5384627

Research Article

Numerical Analysis of Forced Convection of Nanofluid under Turbulent Flow between Two Parallel Plates

Iman Pishkar[1] **and S. Mohammad Hoseini**[2]

[1]*Department of Mechanical Engineering, Payame Noor University (PNU), P.O. Box 19395-4697, Tehran, Iran*
[2]*Shahrekord University of Medical Science, Shahrekord, Iran*

Correspondence should be addressed to Iman Pishkar; iman7449@gmail.com

Received 24 December 2021; Revised 23 May 2022; Accepted 2 June 2022; Published 3 December 2022

Academic Editor: Anum Shafiq

As research shows, in new and renewable energy systems, including solar energy, the study of turbulent flow is of great importance due to its high efficiency in heat transfer. It is also used in petrochemical and oil industries and cooling systems. Therefore, this paper focuses on the turbulent heat transfer of nanofluid between two parallel plates and the effect of the volume fraction of nanoparticles on turbulent heat transfer is investigated. The nanofluid applied in the study was alumina-water. The beginning and the end of the walls were insulated, and the middle part was considered as the heat source. The two-equation κ-ε model was used to model viscosity of turbulent flow. The governing equations were solved simultaneously using the control volume method based on SIMPLER algorithm. In this study, the effects of the Reynolds' number in the range of 10^4 to $5 * 10^4$, volume fraction of 0.01 to 0.04, and nanoparticle diameter of 20 nm to 100 nm on field flow and rate of heat transfer were examined. The influence of Brownian movement on heat performance was considered. Evaluation showed that increasing the Reynolds' number decreased the thickness of the laminar sublayer in turbulent flow and increased temperature and velocity differences. These greater temperature and velocity differences resulted in increased heat transfer and decreased skin friction. The findings imply that heat performance improves when nanoparticles are added to basic fluid. With increasing volume fraction of nanoparticles, shear stress of the channel wall increases, and consequently, skin friction increases too. In addition, the effect of nanoparticle diameter on thermal and hydraulic performance was studied. It was found that heat transfer and skin fraction decreased in the presence of the larger nanoparticles.

1. Introduction

Investigations on forced convection of flow in channels are significant because of their multiple applications in industry, renewable energy systems, and solar energy. Researchers have conducted numerous studies on heat transfer in channels, including Yang et al. [1], Hibachi and Acharya [2] and Tehran and Abed [3] for laminar flow, Vijayan and Bali [4] and Fedora and Visconti [5] for turbulent flow, and Rasool et al. [6–8] for heat transfer of Darcy–Forchheimer nanofluid flow over plates. Krishna and Chamkha [9] studied the heat transfer of micropolar fluid flow past an infinite vertical porous surface. Naseem et al. [10] numerically studied heat transfer in a Newtonian fluid over a porous stretched surface in the presence of constant magnetic and thermal radiation, with considering the role of Dufour and Soret numbers. Ahmed et al. [11] numerically investigated the mixed convective of Williamson fluid flow over a curved surface. Zonta et al. [12] examined the impact on turbulent heat transfer of micro-sized particles dispersed in the flow between two parallel plates. They found the heat flux in walls increases by almost 2% when the flow composed of smaller particles, while the heat transfer is reduced when larger particles are added.

Cooling strategies using fluids with low thermal conductivity limit convection. Nanofluids provide a new environment which causes heat transfer to increase. Thus, nanofluids have many engineering applications, such as cooling systems of electronic components, building heating, solar collector energy storage, nuclear reactor systems, and microbial fuel

cells [13–18]. The effect of using nanofluids on convection heat transfer has been studied by various researchers [19–23]. Nonlinear radiation effects on magnetic/nonmagnetic nanoparticles with different base fluids over a flat plate was studied by Saranya et al. [24]. Heat transfer of different nanofluid flows over a Riga plate was studied by several articles [25–29]. Much research has been carried out related to forced convective heat transfer of nanofluids under laminar flow, for example, the studies by Xu and Pan [30], Tsai and Chein [31], Hedayati and Domairry [32], Malvandi and Ganji [33], and Mirzaei et al. [34]. Santra et al. [35] studied the effect of water-copper nanofluid on heat transfer between two parallel plates under laminar flow. It was shown that when volume fraction of nanoparticles increases, heat transfer increases. Raisi et al. [36] carried out a numerical investigation of thermal performance of microchannels cooled by nanofluid laminar flow of copper and water. In their study, in addition to the Reynolds' number and volume fraction of nanoparticles, the effect of slip factor on the heat transfer rate was studied. Manay and Sahin [37] conducted an experimental study on heat transfer of forced convection in nanofluid laminar flow. The volume fraction of nanofluid and height of the microchannel were found to be important factors on pressure drop and rate of heat transfer in their study. Their results showed that, with increasing microchannel height, heat transfer rate decreased but pressure drop increased.

Numerical and experimental studies have also been carried out on forced convective heat transfer in channels under turbulent flow in nanofluids. Turbulent flow and heat transfer of 3 nanofluids (CuO, SiO_2, and Al_2O_3) in water and ethylene glycol with constant heat flux in a cylindrical pipe were studied by Namburu et al. [38]. They concluded that when volume fraction increases and the diameter of nanoparticles decreases, heat transfer improves. Bianco et al. [39, 40] studied heat transfer of turbulent convection of alumina-water nanofluids in tubes with different boundary conditions. Results showed that the heat transfer coefficient for the nanofluid was greater than that of the fluid and increasing the volume concentration and Reynolds' number the of nanoparticles improved heat performance. Bayat and Nikseresht [41] numerically investigated turbulent nanofluid heat transfer in pipes with constant heat flux boundary conditions. They concluded that when nanoparticle volume fraction increases, heat transfer and pressure drop also increase. Saha and Paul [42] studied turbulent forced convection in horizontal pipes in which the basic fluid was water and the nanoparticles were Al_2O_3 and TiO_2. Increasing the volume fraction of nanoparticles and Reynolds' number and reducing the nanoparticle diameter were found to cause a reduction in the heat transfer rate. Numerical analysis of heat transfer forced convection for turbulent flow of copper-water nanofluid was conducted by Behroyan et al. [43] in a horizontal pipe. This study compared five types of computational fluid dynamics with experimental results of previous studies. Other similar numerical investigations were conducted by Yang et al. [44], Maiga et al. [45], Aghaei et al. [46], and Leong et al. [47].

Williams et al. [48] and Fotukian and Esfahany [49] studied heat transfer of turbulent forced convection of nanofluid in pipes experimentally. Heyhat et al. [50] evaluated heat transfer of horizontal pipes under alumina-water turbulent flow, experimentally. Their experimental results showed that the heat transfer coefficient for a nanofluid is greater than that for a basic fluid and increases by volume concentration of particles. They also found that the effect of Reynolds' number on heat transfer rate is not significant.

Some studies have examined forced convection using non-Newtonian fluids. Usman et al. [51, 52] numerically studied heat transfer of the power-law fluid over and between stretchable rotatory disks. Usman et al. [53] numerically investigated the entropy generation in a power-law nanofluid flow over a stretchable rotatory porous disk. Exploration of temperature dependent thermophysical characteristics of yield exhibiting non-Newtonian fluid flow under gyrotactic microorganisms was studied by Sohail et al. [54]. Heat and mass transmission on mixed convection boundary layer flow of Casson liquid over a linear elongating surface in porous medium was studied by Sohail et al. [55]. They reported that augmenting values of magnetic parameter reduces the fluid velocity and upsurges the temperature and concentration profiles. Sohail and Naz [56] numerically investigated heat and mass transmissions of boundary layer flow of non-Newtonian Sutterby nanofluid by a stretched cylinder by incorporating the revised models by engaging Cattaneo–Christov theory. Mathematical model and rheological aspects of chemically reacting Casson-type nanofluid flow considering ethylene glycol-based nanoparticles with thermophoretic diffusion and Brownian motion was studied by Osman et al. [57]. Shamshuddin and Ghaffari [58] investigated the heat and mass transfer in a steady flow of Sutterby nanofluid over the surface of a stretching wedge.

Apart from these studies on circular channels or tubes, other studies have been carried out on the cross. Hussein et al. [59] evaluated friction coefficient and heat transfer in 3 different segmented surfaces, while Mohammed et al. [60] studied hydraulic and thermal parameters of turbulent nanofluid flow in rib-groove channels numerically. In these studies, the rib-grooves were of different forms and the effect of different parameters, including nanofluid type, volume fraction, nanoparticle dimension, and Reynolds' number, was evaluated. They concluded that the highest rate of heat transfer is associated with rectangular grooves. Ziaei-Rad [61] investigated heat transfer of forced convection for two horizontal and parallel plates under turbulent nanofluid flow of alumina-water. The κ-ε model was used to calculate turbulent viscosity. He found that effect of adding nanoparticles to basic fluid is greater for hydraulic and thermal parameters.

According to recent research, there is a lack of investigation regarding heat transfer of forced convection under turbulent flow of a nanofluid between 2 parallel plates. Despite the heat transfer of pure fluid in forced convection under turbulent flow through two parallel plates and pipes, the heat transfer of nanofluid forced convection has been observed to be lower in these channels. Therefore, we decided to study heat transfer of forced convection of nanofluid between two parallel plates. The thermal conditions imposed in this case have not been observed in previous studies. The effect

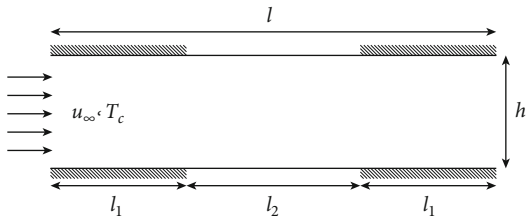

Figure 1: Physical schematic of the problem.

of Brownian motion of nanoparticles on thermal performance is included. The main subject of this study is to evaluate the effect of various parameters of alumina-water nanofluid on thermal and hydraulic performance under turbulent flow. A single-phase model is applied in this study.

2. Problem Description

The schematic of the present problem is shown in Figure 1. A horizontal channel of length l and height h is assumed. Nanofluid flow with constant temperature T_c and horizontal velocity u_∞ enters channel from left and exits from right. The channel is divided into 3 parts: input and output of a channel with length l_1, which is insulated and the middle of the channel is a thermal source with temperature T_h and length of l_2. All mentioned parameters are dimensionless, with channel height (h). Height of channel $H = h/h = 1$, length $L = l/h = 100$, length of entry and output $l_1/h = 25$, and length of middle part $l_2/h = 50$. The present study examines Reynolds' number, volume fraction, and diameter of nanoparticles on flow and heat transfer rate.

3. Formulation of the Problem

In this study, forced convective heat transfer in a two-dimensional Cartesian system is investigated. The nanofluid is Newtonian and incompressible, and the flow is turbulent and steady state. The condition is considered nonslip at the walls. There is a thermal equilibrium between the fluid and the nanoparticles in the channel. The geometry and diameter of nanoparticles are the same. The effect of viscous dissipation is ignored, and there is no generation and storage of energy. The governing equations on turbulent flow, including continuity, momentum, and energy are as follows [62].

Connection equation:

$$\frac{\partial u}{\partial x} + \frac{\partial v}{\partial y} = 0. \tag{1}$$

Momentum equation:

$$\frac{\partial}{\partial x_j}\left(\rho u_i u_j\right) = -\frac{\partial p}{\partial x_i} + \frac{\partial}{\partial x_j}\left(\mu\left(\frac{\partial u_i}{\partial x_j} + \frac{\partial u_j}{\partial x_i}\right) - \rho u_i' u_j'\right). \tag{2}$$

Energy equation:

$$\frac{\partial}{\partial x_j}\left(\rho C_p u_j T\right) = \frac{\partial}{\partial x_j}\left(\lambda\frac{\partial T}{\partial x_j} - \rho C_p u_j' T'\right). \tag{3}$$

To stimulate turbulent flow, the κ-ε two-equation model is used. Equations are presented below for turbulent kinetic energy (κ) and dissipation rate of turbulent kinetic energy (ε), as proposed by Jones and Launder [63].

$$\frac{\partial}{\partial x_j}\left(\rho u_j k\right) = \frac{\partial}{\partial x_j}\left(\left(\mu + \frac{\mu_t}{\sigma_k}\right)\frac{\partial k}{\partial x_j}\right) + \mu_t\frac{\partial u_i}{\partial x_j}\left(\frac{\partial u_i}{\partial x_j} + \frac{\partial u_j}{\partial x_i}\right) - \rho\varepsilon,$$

$$\frac{\partial}{\partial x_j}\left(\rho u_j \varepsilon\right) = \frac{\partial}{\partial x_j}\left(\left(\mu + \frac{\mu_t}{\sigma_\varepsilon}\right)\frac{\partial \varepsilon}{\partial x_j}\right) + C_1\mu_t\frac{\varepsilon}{k}\frac{\partial u_i}{\partial x_j}\left(\frac{\partial u_i}{\partial x_j} + \frac{\partial u_j}{\partial x_i}\right) - C_2\rho\frac{\varepsilon^2}{k}. \tag{4}$$

The constant values of the κ-ε model presented by Launder and Sharma [64] are as follows.

$$C_1 = 1.44,\ C_1 = 1.92,\ C_\mu = 0.09,\ \sigma_k = 1.0,\ \sigma_\varepsilon = 1.3. \tag{5}$$

The terms $\boldsymbol{u_i' u_j'}$ Reynolds' stresses are presented by the Boussinesq assumption as follows [65].

$$-\rho u_i' u_j' = \mu_t\left(\frac{\partial u_i}{\partial x_j} + \frac{\partial u_j}{\partial x_i}\right) - \frac{2}{3}\delta_{ij}\rho\tilde{k}. \tag{6}$$

In addition, the turbulent heat flux $\left(-\rho C_p u_j' T'\right)$ can be written as the turbulent Prandtl number. The turbulent Prandtl number mainly considered here is $\mathrm{Pr_t} = 0.85$.

$$-\rho C_p u_j' T' = \frac{\mu_t C_p}{\mathrm{Pr}_t}\frac{\partial T}{\partial x_j}. \tag{7}$$

Density, heat capacity, volume expansion coefficient, and thermal diffusivity of the nanofluid can be defined as suggested in [66, 67]

$$\begin{aligned}\rho_{\mathrm{nf}} &= (1-\phi)\rho_f + \phi\rho_s,\\ \left(\rho C_p\right)_{\mathrm{nf}} &= (1-\phi)\left(\rho C_p\right)_f + \phi\left(\rho C_p\right)_s,\\ \alpha_{\mathrm{nf}} &= \lambda_{\mathrm{nf}}/\left(\rho C_p\right)_{\mathrm{nf}}.\end{aligned} \tag{8}$$

The Corcoran model was used for thermal conductivity and viscosity of nanofluid. The results of this model were closer to the experimental results. In this model, thermal conductivity and dynamic viscosity depend on temperature, volume fraction of nanofluids, the diameter of the nanoparticles, and thermal conductivity of pure fluids and nanoparticles. The relationships used are according to those presented in [68].

$$\frac{\lambda_{\mathrm{nf}}}{\lambda_{\mathrm{f}}} = 1 + 4.4\,\mathrm{Re}_{\mathrm{p}}^{0.4}\mathrm{Pr}^{0.66}\left(\frac{T}{T_{\mathrm{fr}}}\right)^{10}\left(\frac{\lambda_{\mathrm{p}}}{\lambda_{\mathrm{f}}}\right)^{0.03}\phi^{0.66},$$
$$\frac{\mu_{\mathrm{nf}}}{\mu_{\mathrm{f}}} = \left(1 - 34.87\left(d_{\mathrm{p}}/d_{\mathrm{f}}\right)^{-0.3}\phi^{1.03}\right)^{-1}. \tag{9}$$

The Reynolds' number of nanoparticles and diameter of a water molecule is defined as follows:

$$\mathrm{Re}_{\mathrm{p}} = \frac{2\rho_{\mathrm{f}}k_{\mathrm{b}}T}{\pi\mu_{\mathrm{f}}^2 d_{\mathrm{p}}}, d_{\mathrm{f}} = 0.1\left(\frac{6M}{N\pi\rho_{\mathrm{f}}}\right)^{1/3}. \tag{10}$$

In which, $K_{\mathrm{b}}(k_b = 1.3807 \times 10^{-23} JK^{-1})$ is a fixed value of Boltzmann's constant and $N = 6.0221 \times 10^{23}$ is the Avogadro number in the formulas presented here. $T_{\mathrm{fr}} = 273.16\,\mathrm{K}$ is freezing point and $M = 18.015$ is the molecular weight of the basic fluid. In this model, the effect of Brownian motion of the nanoparticles has been considered. The thermophysical properties of the fluid and Al_2O_3 nanoparticles are presented in Table 1.

With dimensionless equations, a wide range of materials and various streaming modes can be examined in the form of a general problem. We used the following dimensionless variables to obtain the main dimensionless equations.

$$U_i = \frac{u_i}{u_\infty}, X_i = \frac{x_i}{h}, \theta = \frac{T - T_c}{T_h - T_c}, P = \frac{p}{\rho_{nf}u_\infty^2},$$
$$K = \frac{k}{u_\infty^2}, E = \frac{\varepsilon h}{u_\infty^3},$$
$$\mathrm{Re} = \frac{\rho_f u_\infty h}{\mu_f}, \mathrm{Pr} = \frac{\nu_f}{\alpha_f}. \tag{11}$$

The equations of energy, momentum, and continuity were rendered dimensionless by substituting dimensionless parameters, as follows.

Connection equation:

$$\frac{\partial U}{\partial X} + \frac{\partial V}{\partial Y} = 0. \tag{12}$$

X-momentum equation:

$$U\frac{\partial U}{\partial X} + V\frac{\partial U}{\partial Y} = -\frac{\partial}{\partial X}\left(P + \frac{2}{3}K\right) + \frac{\mu_{eff}}{\rho_{nf}\nu_f\,\mathrm{Re}}\left(\frac{\partial^2 U}{\partial X^2} + \frac{\partial^2 U}{\partial Y^2}\right). \tag{13}$$

Y-momentum equation:

$$U\frac{\partial V}{\partial X} + V\frac{\partial V}{\partial Y} = -\frac{\partial}{\partial Y}\left(P + \frac{2}{3}K\right) + \frac{\mu_{\mathrm{eff}}}{\rho_{\mathrm{nf}}\nu_{\mathrm{f}}\,\mathrm{Re}}\left(\frac{\partial^2 V}{\partial X^2} + \frac{\partial^2 V}{\partial Y^2}\right). \tag{14}$$

Table 1: Thermophysical properties of water and nanoparticles [69].

Thermophysical properties	Water	Al_2O_3
$\rho(\mathrm{kgm}^{-3})$	997.1	3970
$C_p(\mathrm{Jkg}^{-1}\mathrm{K}^{-1})$	4179	765
$\lambda(\mathrm{Wm}^{-1}\mathrm{K}^{-1})$	0.613	40
$\nu_f\ (\mathrm{m}^2\mathrm{s}^{-1})$	9.1×10^{-7}	—

Energy equation:

$$U\frac{\partial\theta}{\partial X} + V\frac{\partial\theta}{\partial Y} = \Gamma_T\left(\frac{\partial^2\theta}{\partial X^2} + \frac{\partial^2\theta}{\partial Y^2}\right). \tag{15}$$

κ-ε two-equation model:

$$U\frac{\partial K}{\partial X} + V\frac{\partial K}{\partial Y} = \frac{\Gamma_K}{\rho_{\mathrm{nf}}\nu_f\,\mathrm{Re}}\left(\frac{\partial^2 K}{\partial X^2} + \frac{\partial^2 K}{\partial Y^2}\right) + \frac{1}{\rho_{\mathrm{nf}}\nu_f\,\mathrm{Re}}G_K - E,$$
$$U\frac{\partial E}{\partial X} + V\frac{\partial E}{\partial Y} = \frac{\Gamma_E}{\rho_{nf}\nu_f\,\mathrm{Re}}\left(\frac{\partial^2 E}{\partial X^2} + \frac{\partial^2 E}{\partial Y^2}\right) + \frac{C_1 E}{K\rho_{\mathrm{nf}}\nu_f\,\mathrm{Re}}G_K - C_2\frac{E^2}{K}. \tag{16}$$

In these equations, G_K represents the generation of turbulence kinetic energy due to the mean velocity gradients:

$$G_K = 2\mu_t\left[\left(\frac{\partial U}{\partial X}\right)^2 + \left(\frac{\partial V}{\partial Y}\right)^2\right] + \mu_t\left[\frac{\partial U}{\partial Y} + \frac{\partial V}{\partial X}\right]^2,$$
$$\mu_t = \rho_{\mathrm{nf}}\nu_f\ \mathrm{Re}\ C_\mu\frac{K^2}{E}, \mu_{\mathrm{eff}} = \mu_{\mathrm{nf}} + \mu_t,$$
$$\Gamma_K = \mu_{\mathrm{nf}} + \frac{\mu_t}{\sigma_k}, \Gamma_E = \mu_{\mathrm{nf}} + \frac{\mu_t}{\sigma_\varepsilon}, \Gamma_T = \frac{\alpha_{\mathrm{nf}}}{\alpha_f\,\mathrm{Re}\ \mathrm{Pr}} + \frac{\mu_t}{\rho_{\mathrm{nf}}\nu_f\,\mathrm{Re}\ \mathrm{Pr}_{\mathrm{t}}}. \tag{17}$$

The hydrodynamic boundary conditions of the equations include nonslip condition on the walls and uniform input velocity. The upper and lower walls are insulated, except the middle part of the walls where their temperatures are constant. Output velocity and temperature are developed. The boundary condition for ε at the channel walls follows from the assumption of equivalence between production and dissipation of kinetic energy of the turbulent fluid in the near wall region (see Launder and Spalding for details) [70].

The input of turbulent kinetic energy (κ) and dissipation rate of turbulent kinetic energy (ε) is provided as follows [71].

$$k_{\mathrm{inlet}} = \frac{3}{2}(u_\infty \mathrm{Tu})^2, \varepsilon_{\mathrm{inlet}} = \frac{C_\mu^{0.75}k_{\mathrm{inlet}}^{1.5}}{l_{\mathrm{t}}}. \tag{18}$$

In which the turbulent intensity $\mathrm{Tu} = 0.16(\mathrm{Re})^{-0.125}$ and $l_t = h$, which is the length scale of turbulence.

The boundary conditions for the dimensionless equations are showed in Table 2.

Table 2: Dimensionless boundary conditions.

Walls	Inlet	Outlet
$U = 0$	$U = 0$	$\frac{\partial U}{\partial X} = 0$
$V = 0$	$V = 0$	$\frac{\partial V}{\partial X} = 0$
$\theta = 1$ or $\frac{\partial \theta}{\partial Y} = 0$	$\theta = 0$	$\frac{\partial \theta}{\partial X} = 0$
$K = 0$	$K = \frac{3}{2}(\mathrm{Tu})^2$	$\frac{\partial K}{\partial X} = 0$
$E = \frac{C_\mu^{0.75} K_P^{1.5}}{\kappa Y_P}$	$E = C_\mu^{0.75}\left(\frac{3}{2}\right)^{1.5}(\mathrm{Tu})^3$	$\frac{\partial E}{\partial X} = 0$

P is the nearest point to the wall along the Y axis. The Nusselt number is a parameter that indicates the amount of heat transfer. The local Nusselt number on the hot source is defined as follows [72].

$$\mathrm{Nu}(X) = -\frac{k_{\mathrm{nf}}}{k_{\mathrm{f}}}\frac{\partial \theta}{\partial Y}\bigg|_{Y=0}. \tag{19}$$

By integrating local Nusselt numbers during the flow along the warm part of the wall, the average Nusselt number can obtained as follows:

$$\mathrm{Nu}_{\mathrm{m}} = \frac{1}{L_2}\int_{L_1}^{L_1+L_2} \mathrm{Nu}(X)dX. \tag{20}$$

The local and average skin friction is presented as follows:

$$C_{\mathrm{f}}(X) = \frac{2\tau_{\mathrm{w}}}{\rho u_\infty^2} = \frac{2\mu_{\mathrm{nf}}\partial U/\partial Y|_{Y=0}}{\rho_{\mathrm{nf}}\nu_{\mathrm{f}}\,\mathrm{Re}}, C_{\mathrm{fm}} = \frac{1}{L}\int_0^L C_{\mathrm{f}}(X)dX. \tag{21}$$

4. Numerical Method and Validation

The governing equations and boundary conditions are discretized by the finite difference method based on finite volume. The power-law scheme is used for convection-diffusion terms. The SIMPLER algorithm is used to solve equations simultaneously. First, the velocity equations U, V are solved by initial conjecture and the corrected pressures are obtained. Subsequently, the temperature equations and the turbulent flow equations k-e are solved; the details of which are given in Reference [73]. A computer program was written using FORTRAN programming language to run the algorithm, and the convergence criteria were as follows:

$$\frac{\sum_i^M \sum_j^N \left|\varphi_{i,j}^{r+1} - \varphi_{i,j}^{r}\right|}{\sum_i^M \sum_j^N \left|\varphi_{i,j}^{r+1}\right|} \le 10^{-7}. \tag{22}$$

N and M are nodes of the grid in directions X and Y. φ represents the dimensionless dependent parameters that are solved, and r is the number of repetitions. To ensure

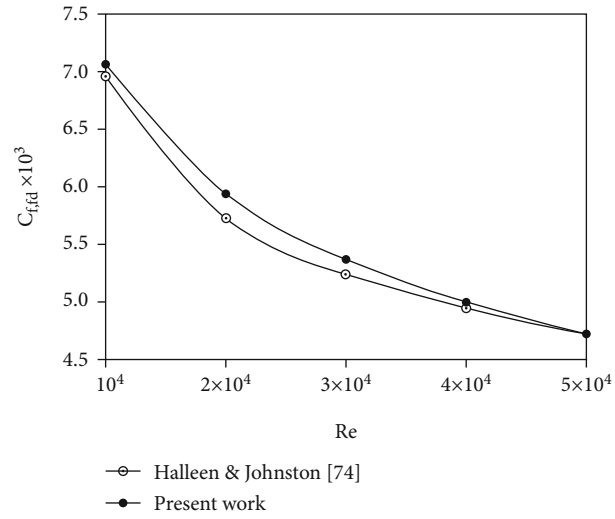

Figure 2: Comparison of skin friction found in the present study with the relationship found by Halleen et al. [74].

Table 3: Comparison between Nusselt numbers found in the present work and those of Hatton and Quarmby [75].

	Hatton and Quarmby [75] $\mathrm{Nu}_{\mathrm{fd}}^*$	Present work $\mathrm{Nu}_{\mathrm{fd}}^*$	Error (%)
Re = 7096, Pr = 1	26	27.054	3.895
Re = 7096, Pr = 10	148	151.623	2.389
Re = 73612, Pr = 1	76.5	78.182	2.151
Re = 73612, Pr = 10	519	532.342	2.506

the accuracy of the written code, it was compared with results presented in previous studies. First, skin friction was compared with the relationship found by Halleen et al. [74]. In this paper, the turbulent flow is investigated experimentally in the channel and the skin friction coefficient is obtained in this way ($C_{f,\mathrm{fd}} = 2\tau_w/\rho u_\infty^2 = 0.0706\,\mathrm{Re}^{-1/4}$. Figure 2 shows the C_f graph at different Reynolds' numbers for a pure fluid. As it turns out, there is little difference between the results.

In addition, for the accuracy of thermal performance, the consistency of the present work with the findings of Hatton and Quarmby [75] was investigated. In their study, the Nusselt number for an area between two parallel plates where one side is insulated and the other is at a constant temperature for various Reynolds' and Prandtl numbers was calculated. According to Table 3, it can be seen that there is little difference between the results and the accuracy of our computer program, which is thus acceptable.

$$\mathrm{Nu}_{\mathrm{fd}}^* = \frac{\left(-\partial T/\partial y|_{y=0}\right)2H}{T_{\mathrm{w}} - T_{\mathrm{m}}}. \tag{23}$$

To perform the computerized calculations, first, a suitable grid should be chosen. Velocity in the turbulent boundary layer is divided in two parts of the viscous sublayer and

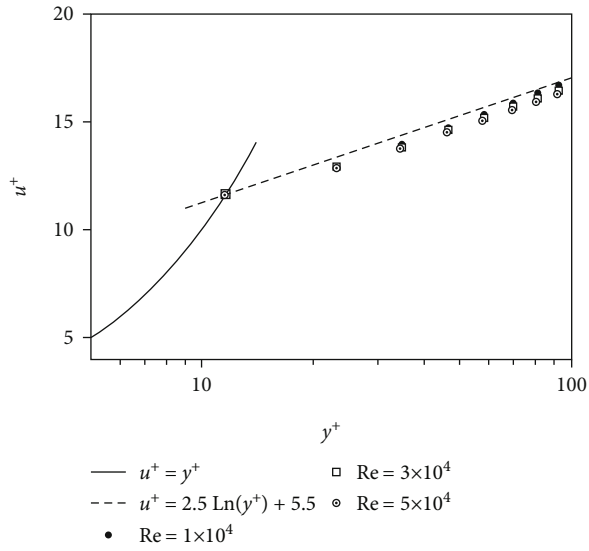

Figure 3: Comparison between values of $u+$ in the present work with Coles and Hirst [76].

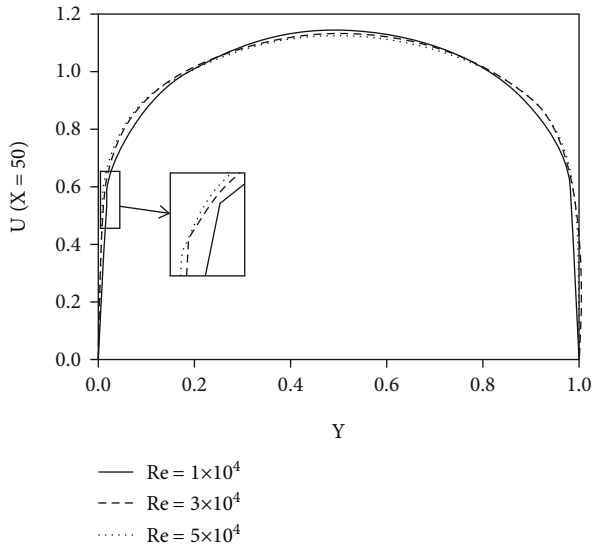

Figure 4: Velocity profile for different Reynolds' numbers.

Table 4: Suitable grid for different Reynolds' numbers.

Re	Suitable grid
$\mathrm{Re} = 10^4$	$400 * 50$
$\mathrm{Re} = 2 \times 10^4$	$400 * 90$
$\mathrm{Re} = 3 \times 10^4$	$400 * 130$
$\mathrm{Re} = 4 \times 10^4$	$400 * 170$
$\mathrm{Re} = 5 \times 10^4$	$400 * 210$

fully turbulent sublayer. Coles and Hirst [76] have modeled velocity in these two parts as follows.

$$u^+ = y^+ \quad y^+ < 11.6,$$
$$u^+ = 2.5 \ln (y^+) + 5.5 \quad y^+ > 11.6. \tag{24}$$

Figure 3 shows values of $u+$ based on $y+$, showing little difference between the results of the present research and the relationships found in Coles and Hirst [76].

$y+$ depends on the one hand on the number of points in the y-direction and on the other hand is dependent on the Reynolds' number. So, for different Reynolds' numbers, $y_P^+ \cong 11.6$ is considered. A suitable grid for different Reynolds' numbers is shown in Table 4.

5. Results and Discussion

After confirming the reliability of the program, we extracted the results. The effect of different parameters, including Reynolds' number ($1 \times 10^4 \le \mathrm{Re} \le 5 \times 10^4$), nanoparticle volume fraction ($0 \le \phi \le 0.04$), and nanoparticle diameter ($20\ \mathrm{nm} \le d_p \le 100\ \mathrm{nm}$) on hydraulic and thermal performance were investigated. Hot wall temperature ($T_\mathrm{h} = 320\ \mathrm{K}$) and cold wall temperature ($T_\mathrm{c} = 295\ \mathrm{K}$) and Prandtl number ($\mathrm{Pr} = 6.2$) were assumed to be constant in the calculations.

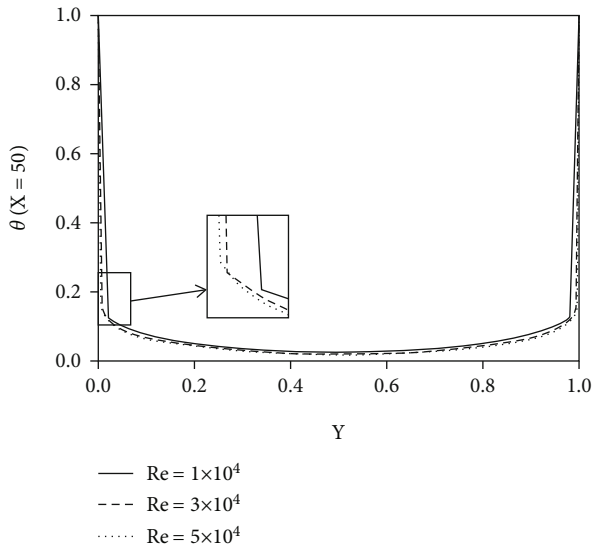

Figure 5: Temperature profile for different Reynolds' numbers.

5.1. Reynolds' Number. It this section, the volume fraction of nanoparticles ($\phi = 0.04$) and diameters of nanoparticles ($d_s = 20\ \mathrm{nm}$) were fixed and the effect of the Reynolds' number was studied. Velocity profiles for different Reynolds' numbers in Figure 4 show that a higher Reynolds' number causes a steeper slope near the wall. Figure 5 shows that by increasing the Reynolds' number the temperature profile slope rises and thus the temperature gradient increases in the boundary layer.

A larger Reynolds' number shows higher entry velocity. Physically, when velocity increases, the convection terms become more significant in the energy equation. Therefore, the heat transfer rate increases. We observe in the temperature

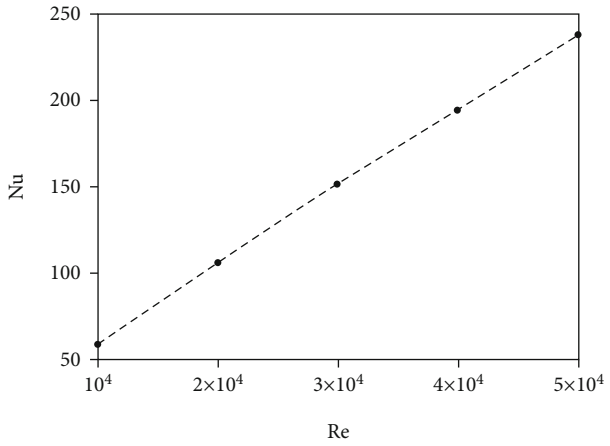

Figure 6: Average Nusselt number variations for different Reynolds' numbers.

graph that when the Reynolds' number increases, temperature gradient increases near the wall. Temperature change has a direct relationship with the average Nusselt number. When temperature gradient increases near the wall, the average Nusselt number also increases. Figure 6 shows average Nusselt number variations for different Reynolds' numbers. In this figure, it is observed that with increasing Reynolds number, heat transfer or Nusselt number has increased. By increasing the Reynolds number, in fact, the speed of the inlet flow to the channel increases, which increases the heat transfer from the surface. In fact, in the energy equation, the convection terms increase, which increases the heat transfer.

The local skin friction coefficient for different Reynolds' numbers is shown in Figure 7. At the entrance of the channel, C_f has maximum value and this reduces until it reaches a fixed amount (hydraulic developed area). As can be seen, with increasing Reynolds' number, C_f has declined. The velocity profiles in Figure 4 show that, with increasing velocity, velocity gradient and therefore the shear stress increase. Moreover, the friction coefficient has an inverse relationship with the input speed or Reynolds' number. On the other hand, the effect of Reynolds' number on the friction coefficient is greater than on the shear stress. Therefore, by increasing the Reynolds' number, the skin friction coefficient is reduced.

5.2. Volume Fraction of Nanoparticles. Due to the impact of volume fraction of nanoparticles on thermophysical properties of nanofluids, it was decided to evaluate this parameter. Here, too, the diameter of the nanoparticles is constant (d_s = 20 nm). Changes in the average skin friction coefficient based on Reynolds' number are shown for different volume fractions in Figure 8. Physically, with increasing the volume fraction of nanoparticles, the wear of nanoparticles with the wall increases, and as a result, the shear stress on the wall increases and skin friction increases.

Values of average Nusselt number and its increase were compared with those for pure fluid for different Reynolds' numbers and different volume fractions, as shown in Table 5.

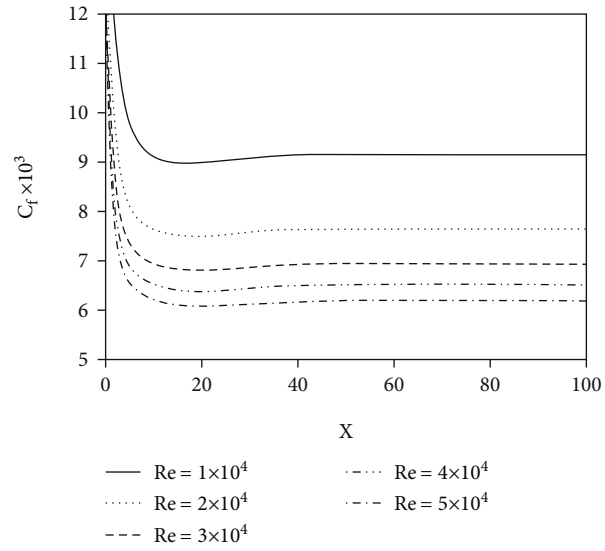

Figure 7: Local skin friction coefficient along the channel.

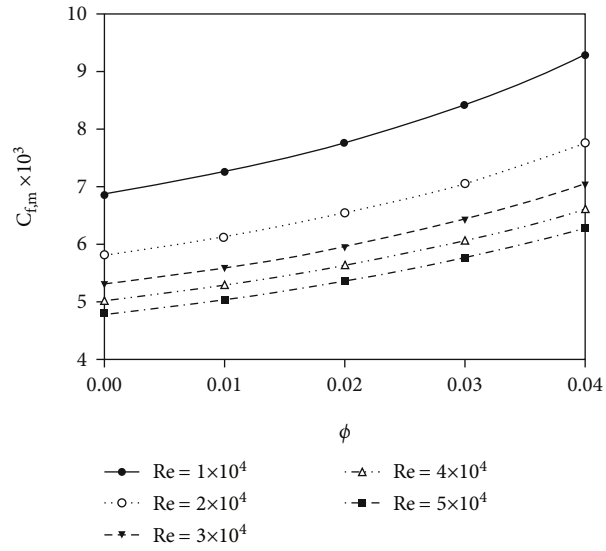

Figure 8: Changes in skin friction based on volume fraction of nanoparticles for different Reynolds' numbers.

According to the results presented in this table, it can be seen that for a fixed volume fraction of nanoparticles with increasing Reynolds' numbers, convection flows are amplified and heat transfer rate increases. By increasing ϕ, the conductivity of nanofluids increases, which increases the heat transfer rate and therefore the average Nusselt number. In addition, Brownian motion effects, applied in the thermal conductivity of a nanofluid, increase the heat transfer rate. Increase in ϕ and Reynolds' number are factors affecting the rate of heat transfer. Adding nanoparticles at high Reynolds' numbers causes heat transfer to increase much more. The reason for this is the faster heat transmission speed in high Reynolds' numbers. In other words, fluid flow captures heat from the heat source more quickly and transfers it to the outlet then cold flows are quickly replaced.

Table 5: Values of average Nusselt and its increase for different Reynolds' numbers and volume fractions.

		$\phi = 0$	$\phi = 0.02$	$\phi = 0.04$
$Re = 1 \times 10^4$	Nu_m	45.869	53.689	58.269
	Increase	0	7.82	12.4
$Re = 2 \times 10^4$	Nu_m	83.429	97.55	105.899
	Increase	0	14.121	22.47
$Re = 3 \times 10^4$	Nu_m	118.876	138.903	150.804
	Increase	0	20.027	31.928
$Re = 4 \times 10^4$	Nu_m	153.987	179.817	195.221
	Increase	0	25.83	41.234
$Re = 5 \times 10^4$	Nu_m	187.295	218.621	237.347
	Increase	0	31.326	50.052

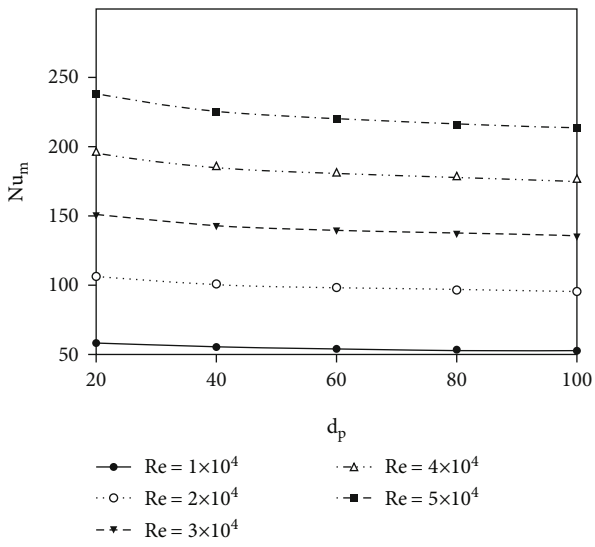

Figure 9: Changes in the average Nusselt number depending on the diameter of the nanoparticles, for different Reynolds' numbers.

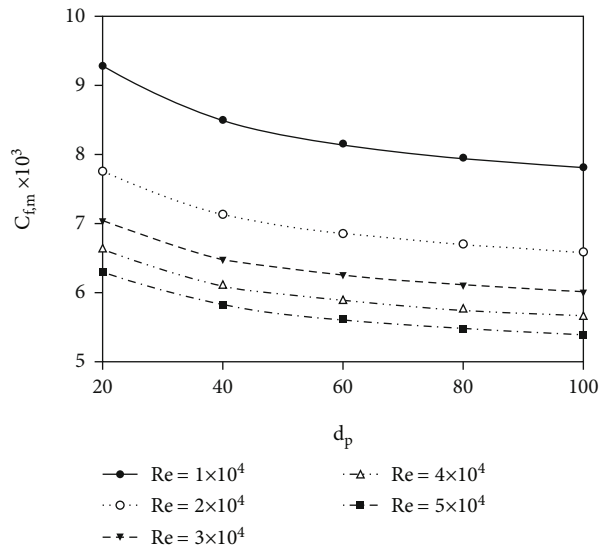

Figure 10: Variations of average skin friction coefficient based on nanoparticle diameter ($\phi = 0.04$).

This increases the temperature gradient, thereby increasing the average Nusselt number.

5.3. Nanoparticle Diameter. The diameter of the nanoparticles affects the viscosity and thermal conductivity of nanofluids. Figure 9 shows the average Nusselt number, depending on the diameter of the nanoparticles, for different Reynolds' numbers. Physically, the smaller the diameter of the nanoparticles, the more the heat transfer rate increases, because the surface area between the nanoparticles and the base fluid increases. In addition, according to the relationship of the thermal conductivity of nanofluids, reducing the diameter of the nanoparticles increases the thermal conductivity and thus the heat transfer rate increases. The larger the Reynolds' number, the greater the effect of particle size on the rate of heat transfer: when Reynolds' number increases, variations in size of the nanoparticles also have a greater effect.

A graph of average skin friction coefficient is shown in Figure 10, based on variation in the diameter of the nanoparticles. When nanoparticle diameter increases, the viscosity of the nanofluid decreases, thereby reducing shear stress. As can be seen in Figure 10, with a constant Reynolds' number, $C_{f,m}$ is reduced with increasing nanoparticle diameter. The laminar sublayer is thicker in turbulent flow when the diameter of the nanoparticles is larger, so the velocity gradient is reduced.

6. Conclusion

The present study evaluated turbulent forced convection heat transfer of an alumina-water nanofluid in a horizontal channel with two fixed constant temperature heaters on each side.

Governing equations were solved using the SIMPLER algorithm. Variations in Reynolds' number, volume fraction, and diameter of nanoparticles were studied. In general, the study of turbulent flow inside the channels gives a better physical view of the flow conditions and close adaptation to the actual state of the flow inside the channel. The results can be summarised as follows:

(a) Higher Reynolds' numbers increase flow rate and reduce laminar sublayer thickness in turbulent flow. Consequently, temperature and velocity gradients increase in this area. Higher Reynolds' numbers increase heat transfer and reduce skin friction coefficient

(b) Increasing the volume fraction of nanoparticles causes the average Nusselt number to increase, and thus, a higher heat transfer rate occurs. For higher Reynolds' numbers, the volume fraction of nanoparticles has a greater effect on heat transfer

(c) When nanoparticles are added to a base fluid, wall shear stress and consequently the skin friction coefficient increase

(d) With smaller diameters of nanoparticles, the contact area of the nanoparticles with the base fluid increases, and the heat transfer ratio becomes greater. Moreover, the skin friction coefficient has a higher value with small diameters

The following topics are suggested to the readers of this article to complete the study: use of other proposed models for the thermophysical properties of nanofluids, the effects of magnetic field on turbulent flow, channel rotation at different angles and the effect of free convection on channel flow, and the application of channels with convergent and divergent geometries.

Nomenclature

C_f: Skin friction
C_p: Specific heat (J/kgK)
E: Dimensionless dissipation rate of turbulent kinetic energy
h: Channel height (m)
H: Dimensionless channel height ($H = h/h = 1$)
K: Dimensionless turbulent kinetic energy
l: Channel length (m)
L: Dimensionless channel length ($L = l/h$)
N: Avogadro number
Nu: Nusselt number
p: Fluid pressure (Pa)
P: Dimensionless pressure
Pr: Prandtl number
Re: Reynolds number
T: Temperature (K)
T_c: Inlet flow temperature (K)
T_h: Thermal source temperature (K)
u, v: Velocity components (m/s)
U, V: Dimensionless velocity components
u_∞: Inlet velocity (m/s).

Greek Symbols

α: Thermal diffusivity (m^2/s)
ε: Dissipation rate of turbulent kinetic energy (m^2/s^3)
θ: Dimensionless temperature
κ: Turbulent kinetic energy (m^2/s^2)
λ: Thermal conductivity (W/mK)
μ: Dynamic viscosity (NS/m^2)
μ_t: Turbulent molecular viscosity
ν: Kinematic viscosity (m^2/s)
ρ: Density (kg/m^3)
φ: Solid volume fraction.

Subscripts

eff: Effective
f: Pure fluid
m: Mean
nf: Nanofluid
s: Nanoparticle.

Data Availability

All required data is available in the text of the paper.

Conflicts of Interest

The authors declare that they have no conflicts of interest.

References

[1] M. H. Yang, R. H. Yeh, and J. J. Hwang, "Mixed convective cooling of a fin in a channel," *International Journal of Heat and Mass Transfer*, vol. 53, no. 4, pp. 760–771, 2010.

[2] S. Habchi and S. Acharya, "Laminar mixed convection in a partially blocked, vertical channel," *International Journal of Heat and Mass Transfer*, vol. 29, no. 11, pp. 1711–1722, 1986.

[3] F. Bazdidi-Tehrani and M. Naderi-Abadi, "Numerical analysis of laminar heat transfer in entrance region of a horizontal channel with transverse fins," *International Communications in Heat and Mass Transfer*, vol. 31, no. 2, pp. 211–220, 2004.

[4] P. Vijayan and C. Balaji, "Turbulent forced convection in a parallel plate channel with natural convection on the outside," *International Communications in Heat and Mass Transfer*, vol. 31, no. 7, pp. 1027–1036, 2004.

[5] A. G. Fedorov and R. Viskanta, "Turbulent natural convection heat transfer in an asymmetrically heated, vertical parallel-plate channel," *International Journal of Heat and Mass Transfer*, vol. 40, no. 16, pp. 3849–3860, 1997.

[6] G. Rasool, T. Zhang, A. J. Chamkha, A. Shafiq, I. Tlili, and G. Shahzadi, "Entropy generation and consequences of binary chemical reaction on MHD Darcy–Forchheimer Williamson nanofluid flow over non-linearly stretching surface," *Entropy*, vol. 22, no. 1, p. 18, 2020.

[7] G. Rasool, A. Shafiq, and D. Baleanu, "Consequences of Soret–Dufour effects, thermal radiation, and binary chemical reaction on Darcy Forchheimer flow of nanofluids," *Symmetry*, vol. 12, no. 9, p. 1421, 2020.

[8] G. Rasool, W. A. Khan, S. M. Bilal, and I. Khan, "MHD squeezed Darcy–Forchheimer nanofluid flow between two h–distance apart horizontal plates," *Open Physics*, vol. 18, no. 1, pp. 1100–1107, 2020.

[9] M. V. Krishna and A. J. Chamkha, "Thermo-diffusion, chemical reaction, Hall and ion slip effects on MHD rotating flow of micro-polar fluid past an infinite vertical porous surface," *International Journal of Ambient Energy*, pp. 1–13, 2021.

[10] T. Naseem, U. Nazir, and M. Sohail, "Contribution of Dufour and Soret effects on hydromagnetized material comprising temperature-dependent thermal conductivity," *Heat Transfer*, vol. 50, no. 7, pp. 7157–7175, 2021.

[11] K. Ahmed, W. A. Khan, T. Akbar, G. Rasool, S. O. Alharbi, and I. Khan, "Numerical investigation of mixed convective Williamson fluid flow over an exponentially stretching permeable curved surface," *Fluids*, vol. 6, no. 7, p. 260, 2021.

[12] F. Zonta, C. Marchioli, and A. Soldati, "Direct numerical simulation of turbulent heat transfer modulation in microdispersed channel flow," *Acta Mechanica*, vol. 195, no. 1-4, pp. 305–326, 2008.

[13] S. P. Jang and S. U. Choi, "Cooling performance of a microchannel heat sink with nanofluids," *Applied Thermal Engineering*, vol. 26, no. 17-18, pp. 2457–2463, 2006.

[14] D. P. Kulkarni, D. K. Das, and R. S. Vajjha, "Application of nanofluids in heating buildings and reducing pollution," *Applied Energy*, vol. 86, no. 12, pp. 2566–2573, 2009.

[15] T. P. Otanicar, P. E. Phelan, R. S. Prasher, G. Rosengarten, and R. A. Taylor, "Nanofluid-based direct absorption solar collector," *Journal of Renewable and Sustainable Energy*, vol. 2, no. 3, p. 033102, 2010.

[16] J. Buongiorno, L. W. Hu, S. J. Kim, R. Hannink, B. A. O. Truong, and E. Forrest, "Nanofluids for enhanced economics and safety of nuclear reactors: an evaluation of the potential features, issues, and research gaps," *Nuclear Technology*, vol. 162, no. 1, pp. 80–91, 2008.

[17] T. Sharma, A. L. M. Reddy, T. S. Chandra, and S. Ramaprabhu, "Development of carbon nanotubes and nanofluids based microbial fuel cell," *International Journal of Hydrogen Energy*, vol. 33, no. 22, pp. 6749–6754, 2008.

[18] X. Fan, H. Chen, Y. Ding, P. K. Plucinski, and A. A. Lapkin, "Potential of 'nanofluids' to further intensify microreactors," *Green Chemistry*, vol. 10, no. 6, pp. 670–677, 2008.

[19] S. Dinarvand, M. Nademi Rostami, R. Dinarvand, and I. Pop, "Improvement of drug delivery micro-circulatory system with a novel pattern of CuO-Cu/blood hybrid nanofluid flow towards a porous stretching sheet," *International Journal of Numerical Methods for Heat & Fluid Flow*, vol. 29, no. 11, pp. 4408–4429, 2019.

[20] S. M. Mousavi, M. N. Rostami, M. Yousefi, S. Dinarvand, I. Pop, and M. A. Sheremet, "Dual solutions for Casson hybrid nanofluid flow due to a stretching/shrinking sheet: a new combination of theoretical and experimental models," *Chinese Journal of Physics*, vol. 71, pp. 574–588, 2021.

[21] S. Dinarvand and M. Nademi Rostami, "An innovative mass-based model of aqueous zinc oxide–gold hybrid nanofluid for von Kármán's swirling flow," *Journal of Thermal Analysis and Calorimetry*, vol. 138, no. 1, pp. 845–855, 2019.

[22] M. Aghamajidi, M. E. Yazdi, S. Dinarvand, and I. Pop, "Tiwari-Das nanofluid model for magnetohydrodynamics (MHD) natural-convective flow of a nanofluid adjacent to a spinning down-pointing vertical cone," *Propulsion and Power Research*, vol. 7, no. 1, pp. 78–90, 2018.

[23] S. Dinarvand, "Nodal/saddle stagnation-point boundary layer flow of CuO–Ag/water hybrid nanofluid: a novel hybridity model," *Microsystem Technologies*, vol. 25, no. 7, pp. 2609–2623, 2019.

[24] S. Saranya, P. Ragupathi, B. Ganga, R. P. Sharma, and A. K. Abdul Hakeem, "Non-linear radiation effects on magnetic/non-magnetic nanoparticles with different base fluids over a flat plate," *Advanced Powder Technology*, vol. 29, no. 9, pp. 1977–1990, 2018.

[25] P. Ragupathi, S. Saranya, A. K. Abdul Hakeem, and B. Ganga, "Numerical analysis on the three-dimensional flow and heat transfer of multiple nanofluids past a Riga plate," in *Journal of Physics: Conference Series*, vol. 1850, no. 1, p. 12044, 2021.

[26] A. K. Abdul Hakeem, P. Ragupathi, S. Saranya, and B. Ganga, "Three dimensional non-linear radiative nanofluid flow over a Riga plate," *Journal of Applied and Computational Mechanics*, vol. 6, no. 4, pp. 1012–1029, 2020.

[27] A. K. Hakeem, P. Ragupathi, B. Ganga, and S. Nadeem, "Three-dimensional viscous dissipative flow of nanofluids over a Riga plate," *Journal of Heat and Mass Transfer Research*, vol. 8, no. 1, pp. 49–60, 2021.

[28] P. Ragupathi, A. K. Abdul Hakeem, S. Saranya, and B. Ganga, "Non-Darcian three-dimensional flow of Fe3O4/Al2O3 nanoparticles with H2O/NaC6H9O7 base fluids past a Riga plate embedded in a porous medium," *The European Physical Journal Special Topics*, vol. 228, no. 12, pp. 2571–2600, 2019.

[29] P. Ragupathi, A. K. A. Hakeem, Q. M. al-Mdallal, B. Ganga, and S. Saranya, "Non-uniform heat source/sink effects on the three-dimensional flow of Fe_3O_4 /Al_2O_3 nanoparticles with different base fluids past a Riga plate," *Case Studies in Thermal Engineering*, vol. 15, p. 100521, 2019.

[30] D. Xu and L. Pan, "Numerical study of nanofluid flow and heat transfer in microchannels," *International Journal of Nanoscience*, vol. 5, no. 6, pp. 747–752, 2006.

[31] T. H. Tsai and R. Chein, "Performance analysis of nanofluid-cooled microchannel heat sinks," *International Journal of Heat and Fluid Flow*, vol. 28, no. 5, pp. 1013–1026, 2007.

[32] F. Hedayati and G. Domairry, "Nanoparticle migration effects on fully developed forced convection of TiO_2-water nanofluid in a parallel plate microchannel," *Particuology*, vol. 24, pp. 96–107, 2016.

[33] A. Malvandi and D. D. Ganji, "Effects of nanoparticle migration on force convection of alumina/water nanofluid in a cooled parallel-plate channel," *Advanced Powder Technology*, vol. 25, no. 4, pp. 1369–1375, 2014.

[34] M. Mirzaei, M. Saffar-Avval, and H. Naderan, "Heat transfer investigation of laminar developing flow of nanofluids in a microchannel based on Eulerian-Lagrangian approach," *The Canadian Journal of Chemical Engineering*, vol. 92, no. 6, pp. 1139–1149, 2014.

[35] A. K. Santra, S. Sen, and N. Chakraborty, "Study of heat transfer due to laminar flow of copper-water nanofluid through two isothermally heated parallel plates," *International Journal of Thermal Sciences*, vol. 48, no. 2, pp. 391–400, 2009.

[36] A. Raisi, B. Ghasemi, and S. M. Aminossadati, "A numerical study on the forced convection of laminar nanofluid in a microchannel with both slip and no-slip conditions," *Numerical Heat Transfer, Part A: Applications*, vol. 59, no. 2, pp. 114–129, 2011.

[37] E. Manay and B. Sahin, "The effect of microchannel height on performance of nanofluids," *International Journal of Heat and Mass Transfer*, vol. 95, pp. 307–320, 2016.

[38] P. K. Namburu, D. K. Das, K. M. Tanguturi, and R. S. Vajjha, "Numerical study of turbulent flow and heat transfer characteristics of nanofluids considering variable properties," *International Journal of Thermal Sciences*, vol. 48, no. 2, pp. 290–302, 2009.

[39] V. Bianco, O. Manca, and S. Nardini, "Entropy generation analysis of turbulent convection flow of Al_2O_3-water nanofluid in a circular tube subjected to constant wall heat flux," *Energy Conversion and Management*, vol. 77, pp. 306–314, 2014.

[40] V. Bianco, O. Manca, and S. Nardini, "Numerical simulation of water/Al_2O_3nanofluid turbulent convection," *Advances in Mechanical Engineering*, vol. 2, 2010.

[41] J. Bayat and A. H. Nikseresht, "Thermal performance and pressure drop analysis of nanofluids in turbulent forced convective flows," *International Journal of Thermal Sciences*, vol. 60, pp. 236–243, 2012.

[42] G. Saha and M. C. Paul, "Numerical analysis of the heat transfer behaviour of water based Al_2O_3 and TiO_2 nanofluids in a circular pipe under the turbulent flow condition," *International Communications in Heat and Mass Transfer*, vol. 56, pp. 96–108, 2014.

[43] I. Behroyan, P. Ganesan, S. He, and S. Sivasankaran, "Turbulent forced convection of Cu-water nanofluid: CFD model comparison," *International Communications in Heat and Mass Transfer*, vol. 67, pp. 163–172, 2015.

[44] Y. Na, T. J. Hanratty, and Z. C. Liu, "The use of DNS to define stress producing events for turbulent flow over a smooth wall," *Flow, Turbulence and Combustion*, vol. 66, no. 4, pp. 495–512, 2001.

[45] S. E. B. Maïga, C. T. Nguyen, N. Galanis, G. Roy, T. Maré, and M. Coqueux, "Heat transfer enhancement in turbulent tube flow using Al_2O_3 nanoparticle suspension," *International Journal of Numerical Methods for Heat & Fluid Flow*, vol. 16, no. 3, pp. 275–292, 2006.

[46] A. Aghaei, G. A. Sheikhzadeh, M. Dastmalchi, and H. Forozande, "Numerical investigation of turbulent forced-convective heat transfer of Al_2O_3-water nanofluid with variable properties in tube," *Ain Shams Engineering Journal*, vol. 6, no. 2, pp. 577–585, 2015.

[47] K. Y. Leong, R. Saidur, T. M. I. Mahlia, and Y. H. Yau, "Entropy generation analysis of nanofluid flow in a circular tube subjected to constant wall temperature," *International Communications in Heat and Mass Transfer*, vol. 39, no. 8, pp. 1169–1175, 2012.

[48] W. Williams, J. Buongiorno, and L. W. Hu, "Experimental investigation of turbulent convective heat transfer and pressure loss of alumina/water and zirconia/water nanoparticle colloids (nanofluids) in horizontal tubes," *Journal of Heat Transfer*, vol. 130, no. 4, 2008.

[49] S. M. Fotukian and M. N. Esfahany, "Experimental investigation of turbulent convective heat transfer of dilute γ-Al_2O_3/water nanofluid inside a circular tube," *International Journal of Heat and Fluid Flow*, vol. 31, no. 4, pp. 606–612, 2010.

[50] M. M. Heyhat, F. Kowsary, A. M. Rashidi, S. A. V. Esfehani, and A. Amrollahi, "Experimental investigation of turbulent flow and convective heat transfer characteristics of alumina water nanofluids in fully developed flow regime," *International Communications in Heat and Mass Transfer*, vol. 39, no. 8, pp. 1272–1278, 2012.

[51] W. K. Usman, I. A. Badruddin, A. Ghaffari, and H. M. Ali, "Heat transfer in steady slip flow of tangent hyperbolic fluid over the lubricated surface of a stretchable rotatory disk," *Case studies in Thermal Engineering*, vol. 24, p. 100825, 2021.

[52] P. L. Usman and A. Ghaffari, "Steady flow and heat transfer of the power-law fluid between two stretchable rotating disks with non-uniform heat source/sink," *Journal of Thermal Analysis and Calorimetry*, vol. 146, no. 4, pp. 1735–1749, 2021.

[53] A. G. Usman, I. Mustafa, T. Muhammad, and Y. Altaf, "Analysis of entropy generation in a power-law nanofluid flow over a stretchable rotatory porous disk," *Case studies in Thermal Engineering*, vol. 28, article 101370, 2021.

[54] M. Sohail, R. Naz, Z. Shah, P. Kumam, and P. Thounthong, "Exploration of temperature dependent thermophysical characteristics of yield exhibiting non-Newtonian fluid flow under gyrotactic microorganisms," *AIP Advances*, vol. 9, no. 12, p. 125016, 2019.

[55] M. Sohail, R. Naz, and S. I. Abdelsalam, "Application of non-Fourier double diffusions theories to the boundary-layer flow of a yield stress exhibiting fluid model," *Physica A: Statistical Mechanics and its Applications*, vol. 537, p. 122753, 2020.

[56] M. Sohail and R. Naz, "Modified heat and mass transmission models in the magnetohydrodynamic flow of Sutterby nanofluid in stretching cylinder," *Physica A: Statistical Mechanics and its Applications*, vol. 549, p. 124088, 2020.

[57] P. Lin and A. Ghaffari, "Heat and mass transfer in a steady flow of Sutterby nanofluid over the surface of a stretching wedge," *Physica Scripta*, vol. 96, no. 6, p. 065003, 2021.

[58] M. D. Shamshuddin, A. Ghaffari, and Usman, "Radiative heat energy exploration on Casson-type nanoliquid induced by a convectively heated porous plate in conjunction with thermophoresis and Brownian movements," *International Journal of Ambient Energy*, pp. 1–12, 2022.

[59] A. M. Hussein, K. V. Sharma, R. A. Bakar, and K. Kadirgama, "The effect of cross sectional area of tube on friction factor and heat transfer nanofluid turbulent flow," *International Communications in Heat and Mass Transfer*, vol. 47, pp. 49–55, 2013.

[60] H. A. Mohammed, A. N. Al-Shamani, and J. M. Sheriff, "Thermal and hydraulic characteristics of turbulent nanofluids flow in a rib- groove channel," *International Communications in Heat and Mass Transfer*, vol. 39, no. 10, pp. 1584–1594, 2012.

[61] M. Ziaei-Rad, "Numerical investigation of pressure drop and heat transfer in developing laminar and turbulent nanofluid flows," *Physica Scripta*, vol. T155, p. 014021, 2013.

[62] S. M. Ghiaasiaan, *Convective Heat and Mass Transfer*, Cambridge University Press, Cambridge, United Kingdom, 2012.

[63] W. P. Jones and B. E. Launder, "The prediction of laminarization with a two-equation model of turbulence," *International Journal of Heat and Mass Transfer*, vol. 15, no. 2, pp. 301–314, 1972.

[64] B. E. Launder and B. I. Sharma, "Application of the energy-dissipation model of turbulence to the calculation of flow near a spinning disc," *Letters in Heat and Mass Transfer*, vol. 1, no. 2, pp. 131–137, 1974.

[65] D. C. Wilcox, *Turbulence modeling for CFD*, vol. 2, DCW Industries, La Canada, CA, 1998.

[66] J. Kim, Y. T. Kang, and C. K. Choi, "Analysis of convective instability and heat transfer characteristics of nanofluids," *Physics of Fluids*, vol. 16, no. 7, pp. 2395–2401, 2004.

[67] A. Raisi, "Heat transfer in an enclosure filled with a nanofluid and containing a heat- generating conductive body," *Applied Thermal Engineering*, vol. 110, pp. 469–480, 2017.

[68] M. Corcione, "Empirical correlating equations for predicting the effective thermal conductivity and dynamic viscosity of nanofluids," *Energy Conversion and Management*, vol. 52, no. 1, pp. 789–793, 2011.

[69] M. Pourabdian, M. Qate, M. R. Morad, and A. Javareshkian, "The Jeffery-Hamel flow and heat transfer of nanofluids by

homotopy perturbation method and comparison with numerical results," 2016, https://arxiv.org/abs/1601.05298.

[70] B. E. Launder and D. B. Spalding, "The numerical computation of turbulent flows," in *Numerical prediction of flow, heat transfer, turbulence and combustion*, pp. 96–116, Pergamon, 1983.

[71] A. Bardow, C. H. Bischof, H. M. Bücker et al., "Sensitivity-based analysis of the k-ε model for the turbulent flow between two plates," *Chemical Engineering Science*, vol. 63, no. 19, pp. 4763–4775, 2008.

[72] A. Raisi, S. M. Aminossadati, and B. Ghasemi, "An innovative nanofluid-based cooling using separated natural and forced convection in low Reynolds flows," *Journal of the Taiwan Institute of Chemical Engineers*, vol. 62, pp. 259–266, 2016.

[73] S. V. Patankar, *Numerical Heat Transfer and Fluid Flow*, CRC Press, Boca Raton, 1980.

[74] J. P. Johnston, R. M. Halleent, and D. K. Lezius, "Effects of spanwise rotation on the structure of two-dimensional fully developed turbulent channel flow," *Journal of Fluid Mechanics*, vol. 56, no. 3, pp. 533–557, 1972.

[75] A. P. Hatton and A. Quarmby, "The effect of axially varying and unsymmetrical boundary conditions on heat transfer with turbulent flow between parallel plates," *International Journal of Heat and Mass Transfer*, vol. 6, no. 10, pp. 903–914, 1963.

[76] D. Coles and E. A. Hirst, "Proceedings computation of turbulent boundary layers," *AFOSRIFP-Stanford Conference*, vol. 2, pp. , 196947–54, 1969.